



Comparative enantioseparation of planar chiral ferrocenes on polysaccharide-based chiral stationary phases

Alessandro Dessì¹ | Barbara Sechi¹ | Roberto Dallochio¹ |
 Bezhn Chankvetadze²  | Mireia Pérez-Baeza³ | Sergio Cossu⁴ |
 Victor Mamane⁵ | Patrick Pale⁵ | Paola Peluso¹ 

¹Istituto di Chimica Biomolecolare ICB, CNR, Sassari, Italy

²Institute of Physical and Analytical Chemistry, School of Exact and Natural Sciences, Tbilisi State University, Tbilisi, Georgia

³Departamento de Química Analítica, Universitat de València, València, Spain

⁴Dipartimento di Scienze Molecolari e Nanosistemi DSMN, Università Ca' Foscari Venezia, Venice, Italy

⁵Institut de Chimie de Strasbourg, UMR CNRS 7177, Equipe LASYROC, Strasbourg Cedex, France

Correspondence

Paola Peluso, Istituto di Chimica Biomolecolare ICB CNR, sede secondaria di Sassari, Traversa La Crucca, 3, Regione Balduca, I-07100 Li Punti, Sassari, Italy. Email: paola.peluso@cnr.it

Victor Mamane, Institut de Chimie de Strasbourg, UMR CNRS 7177, Equipe LASYROC, 1 rue Blaise Pascal, 67008, Strasbourg Cedex, France. Email: vmamane@unistra.fr

Funding information

European Social Fund, Grant/Award Number: BEFPI/2021/073; Generalitat Valenciana, Grant/Award Number: ACIF/2019/158; Centre national de la recherche scientifique; University of Strasbourg; Consiglio Nazionale delle Ricerche

Abstract

Planar chiral ferrocenes are well-known compounds that have attracted interest for application in synthesis, catalysis, material science, and medicinal chemistry for several decades. In spite of the fact that asymmetric synthesis procedures for obtaining enantiomerically enriched ferrocenes are available, sometimes, the accessible enantiomeric excess of the chiral products is unsatisfactory. In such cases and for resolution of racemic planar chiral ferrocenes, enantioselective high-performance liquid chromatography (HPLC) on polysaccharide-based chiral stationary phases (CSPs) has been used in quite a few literature articles. However, although moderate/high enantioselectivities have been obtained for planar chiral ferrocenes bearing polar substituents, the enantioseparation of derivatives containing halogens, or exclusively alkyl groups, remains rather challenging. In this study, the enantioseparation of ten planar chiral 1,2- and 1,3-disubstituted ferrocenes was explored by using five polysaccharide-based CSPs under multimodal elution conditions. Baseline enantioseparations were achieved for nine analytes with separation factors (α) ranging from 1.20 to 2.92. The presence of π -extended systems in the analyte structure was shown to impact affinity of the most retained enantiomer toward amylose-based selectors, observing retention times higher than 80 min with methanol-containing mobile phases (MPs). Electrostatic potential (V) analysis and molecular dynamics (MD) simulations were used in order to study interaction modes at the molecular level.

KEYWORDS

electrostatic potential, enantioseparation, ferrocenes, planar chirality, polysaccharide-based chiral stationary phases

Alessandro Dessì and Barbara Sechi contributed equally to this work.

[This article is part of the Special Issue: A Special Issue to Celebrate the 80th Birthday of Professor Yoshio Okamoto. See the first articles for this special issue previously published in Volumes 33:12, 34:1, 34:2, and 34:3. More special articles will be found in this issue as well as in those to come.]

1 | INTRODUCTION

Ferrocene ($[\text{Fe}(\eta^5\text{-C}_5\text{H}_5)_2]$) is an iconic framework in organometallic chemistry,¹ which, in 1952, was characterized as the first sandwich compound by Woodward et al.² Structurally, ferrocene is a rigid three-dimensional unit wherein iron is located between two cyclopentadienyl (Cp) rings. Owing to its stability and the possibility of functionalization at the Cp rings,^{3–7} ferrocene derivatives have over time found application in several fields such as catalysis,^{8–10} medicinal chemistry,¹¹ and material chemistry.^{12–14} Moreover, the ferrocenium/ferrocene system (Fc^+/Fc) is a versatile redox couple which have proven to be suitable for the preparation of switchable functional systems.^{1,15,16}

Due to their versatility to access molecular wires and responsive switchable systems and materials,^{17–19} particular attention has been devoted to the so-called “ π -extended ferrocenyl frameworks,” which are featured by delocalized orbital networks based on the combination of a ferrocene unit and a π -conjugated extended cloud, such as the ethynyl group.^{13,20} Planar chiral aryl ethynyl ferrocenes have been used as intermediates for the preparation of helical ferrocenes showing peculiar chiroptical properties with very high optical value and huge intensity of the circular dichroism signals.²¹

Recently, our groups developed the design, synthesis, and characterization of compounds **1–8** as new chiral iodoethynyl ferrocenes showing three key features (Figure 1):⁶ (a) planar chirality due to the presence of two different substituents on the same Cp ring, (b) a π -extended ethynyl ferrocenyl moiety, with the possibility to further extend the π -conjugation to the second Cp-substituent depending on its electronic features (Figure 2A,B), and (c) an iodine substituent, as an electrophilic σ -hole donor activated by the $\text{C}\equiv\text{C}$ group (Figure 2D).^{22,23} In this regard, it is worth mentioning that halogen bonds (XBs) were identified in the crystal packing of compounds **1**, **3–5**, and **7** with both lengths

and angles falling within the range of values typically observed for this type of σ -hole bonds.⁶

These features also make compounds **1–8** suitable as test probes to explore the impact of both π -extended clouds and electrophilic σ -holes in enantioselective processes occurring in high-performance liquid chromatography (HPLC) environment, with the aim to profile noncovalent interactions involved in the enantioselective recognition. In previous studies, we demonstrated that σ -hole interactions, such as XBs and chalcogen bonds (ChBs), which involve electrophilic regions of electron charge density depletion (σ -holes), may participate in the enantioselective interaction between polysaccharide-based selectors and selectands containing electrophilic σ -holes.^{24–27}

On this basis, we studied the enantioseparation of chiral ferrocenes **1–8** along with **9** and **10**, as reference compounds for comparison, by using five polysaccharide carbamate-based chiral stationary phases (CSPs) (Table S1). The versatility of polysaccharide-based selectors allowed to explore different interaction modes under multimodal elution conditions by using *n*-hexane (Hex)-based mixtures, pure methanol (MeOH), and aqueous mixtures as mobile phases (MPs). The experiments were integrated with computational analysis by using electrostatic potential (*V*) calculations and molecular dynamics (MD) simulations in order to disclose the mechanistic features of these enantioseparations.

The second aim of this study was to identify suitable methods for baseline enantioseparation of chiral ferrocenes containing small or nonpolar groups. Indeed, although moderate/high enantioselectivities have been obtained with Hex-based mixtures for planar chiral ferrocenes bearing hydroxyl, carbonyl, and carboxyl groups as substituents,^{21,28–30} the enantioseparations reported for derivatives containing small groups, halogens, or exclusively alkyl groups are rather unsatisfying.^{31,32} It is worth mentioning that few papers have reported systematic studies on enantioseparation of organometallic compounds on polysaccharide-based CSPs so far.^{28,31–39}

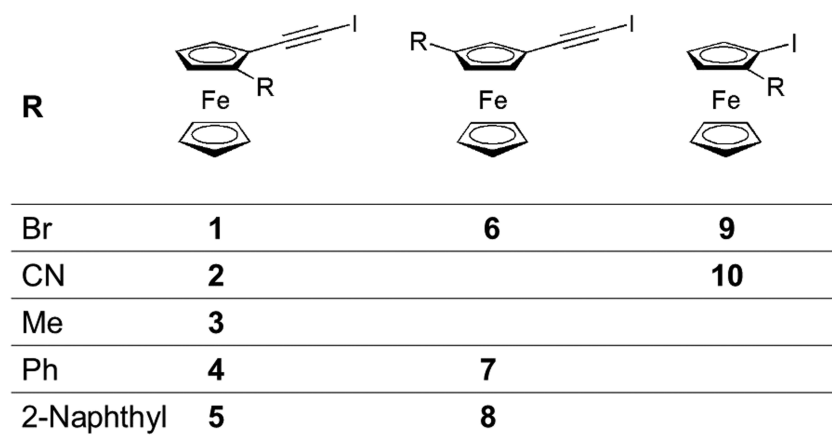
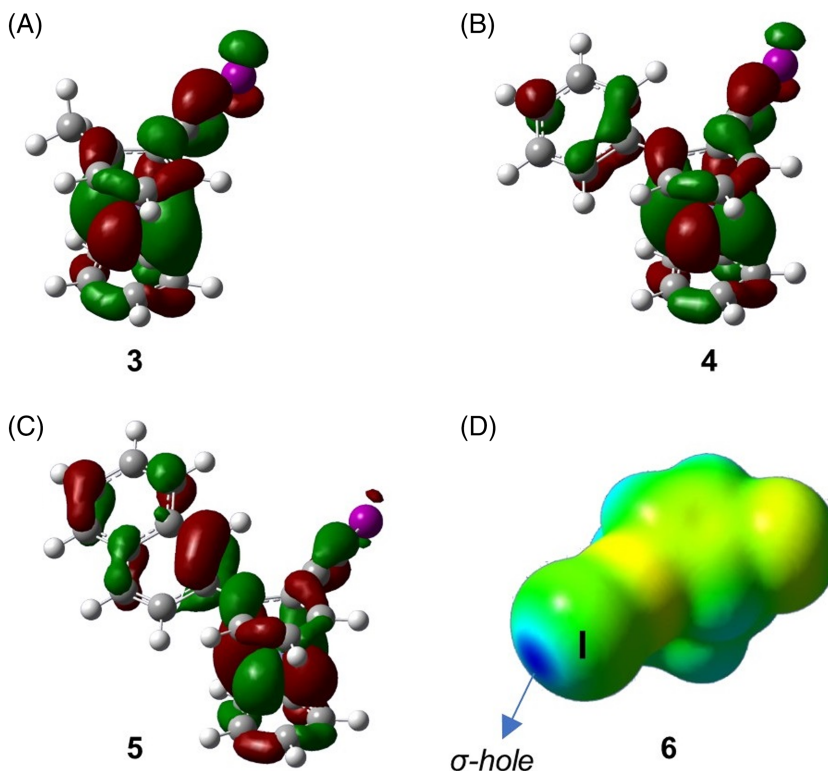


FIGURE 1 Structures and numbering of chiral ferrocenes **1–10**

FIGURE 2 The highest occupied molecular orbitals (HOMO) (contour value = 0.02 au) for compounds **3–5** (A–C) and electrostatic potential isosurface (V_S) (isovalue 0.002 au) of compound **6** (D) (DFT/B3LYP/def2TZVPP; color legend: minimum and maximum V_S values are depicted in red and blue, respectively, and colors in between (orange, yellow, green) depict intermediate values)



2 | MATERIALS AND METHODS

2.1 | Chemicals and reagents

Compounds **1–10** were prepared and characterized as previously reported.^{6,40} HPLC grade Hex, MeOH, 2-propanol (2-PrOH), acetonitrile (ACN), and water were purchased from Sigma-Aldrich (Taufkirchen, Germany).

2.2 | Chromatography

An Agilent Technologies (Waldbronn, Germany) 1100 Series HPLC system (high-pressure binary gradient system equipped with a diode-array detector operating at multiple wavelengths [220, 254, 280, and 360 nm], a programmable autosampler with a 20- μ l loop, and a thermostated column compartment) was employed. Data acquisition and analyses were carried out with Agilent Technologies ChemStation Version B.04.03 chromatographic data software. The UV absorbance is reported as milliabsorbance units (mAU). Lux Cellulose-1 (C-1) (cellulose *tris*(3,5-dimethylphenylcarbamate), CDMPC), Lux *i*-Cellulose-5 (iC-5) (cellulose *tris*(3,5-dichlorophenylcarbamate), CDCPC), Lux Amylose-1 (A-1) and Lux *i*-Amylose-1 (iA-1) (amylose *tris*(3,5-dimethylphenylcarbamate), ADMPC), and Lux

i-Amylose-3 (iA-3) (amylose *tris*(3-chloro-5-methylphenylcarbamate), ACMPC) (5 μ m) (Phenomenex Inc., Torrance, CA, USA) were used as chiral columns (250 \times 4.6 mm) (Table S1). Analyses were performed in isocratic mode at 25°C. The flow rate (FR) was set at 0.8 ml/min. For compounds **1** and **3–8**, the enantiomer elution order (EEO) was determined by injecting enantiomers of known absolute configuration prepared by asymmetric syntheses.⁶ For compounds **9** and **10**, the relative EEO was assigned by injecting pure enantiomers of unknown absolute configuration, which are denoted as X_9 , Y_9 and X_{10} , Y_{10} .

2.3 | Computations

V extrema calculated on the molecular electron density isosurfaces (maxima and minima) ($V_{S,max}$ and $V_{S,min}$) (au, electrons/bohr) were computed by using Gaussian 09 (Wallingford, CT 06492, USA),⁴¹ at the density functional theory (DFT) level of theory, using the B3LYP functional and the def2TZVPP basis set. Search for the exact location of $V_{S,max}$ and $V_{S,min}$ was made through the Multiwfn code⁴² and through its module enabling quantitative analyses of molecular surfaces (isovalue 0.002 au).⁴³ In our computations, .wfn files were obtained through the Gaussian 09 package. Details for MD are reported in the Supporting Information file.

3 | RESULTS AND DISCUSSION

3.1 | Chromatographic screening

In the frame of this study, analytes, CSP, and MP were considered as experimental variables, examined individually, and their influence on retention and selectivity was examined through the evaluation of retention (k) and separation factors (α), on the basis of the following preliminary remarks:

1. Within the 1,2-disubstituted **1–5** and 1,3-disubstituted **6–8** series, the influence of the distinctive functional group on enantioseparation was evaluated. As shown in Figure 2, different substituents on the Cp ring may determine different degrees of delocalization across the entire system. For instance, for compounds **4** (Ph) and **5** (2-Naphth) (Figure 2B,C), the delocalization is across the entire molecule, whereas for compound **3**, the calculated highest occupied molecular orbital (HOMO) does not extend on the second substituent (Me) (Figure 2A). The impact of the triple bond on the enantioseparation was examined, and for this purpose, compounds **9** and **10** served as reference systems for comparison. The effect of 1,2- and 1,3-disubstitution on the enantioseparation was also considered. The local electron charge density of specific molecular regions of the analytes was inspected in terms of calculated V_S (Table S2), positive and negative V_S values being associated with electrophilic and nucleophilic regions;
2. The performances of different polysaccharide selectors were evaluated under multimodal elution conditions and compared in terms of polysaccharide backbone (cellulose-based C-1 vs. amylose-based A-1) and type of carbamate pendant groups (methylated A-1, iA-1, and C-1, chlorinated iC-5, and methylated and chlorinated iA-3). In this regard, the electronic properties of the carbamate moiety, which are tuned by methyl and chlorine substituents located on the phenyl ring of the carbamate pendant groups, were determined by DFT calculations (Table 1). The impact of the anchoring

technique (immobilization vs. coating)^{44,45} was also considered by comparing the performances of ADMPC-based columns (A-1 vs. iA-1);

3. The effect of MP on the enantioseparations was evaluated comparatively under multimodal elution conditions by using *n*-hexanic mixtures (Hex/2-PrOH 95:5 (A) and Hex/2-PrOH/MeOH 95:2.5:2.5 (B) v/v), polar organic (PO) conditions (MeOH 100% (C)), and aqueous-organic mixtures (MeOH/water 95:5 (D) and 90:10 (E) v/v). In particular, the comparative use of A–E, as MPs, allowed for evaluating the effect of increasing hydrophobicity of the medium. The introduction in the MP of 2.5% MeOH (B) allows fine-tuning of the binding between analyte and polysaccharide-based selector by favoring a better penetration of the analyte into the groove and tuning hydrophobic versus hydrogen bond (HB) interactions,^{46,47} while keeping rather unaffected the high-ordered three-dimensional structure of the polysaccharide. Otherwise, the use of pure MeOH (C), as MP, impacts intramolecular HBs determining the high-ordered structure of the polysaccharide, thus producing a huge effect within the polysaccharide structure.^{46–49} In particular, the hydroxyl groups of MeOH molecules strongly interact, as HB donors/acceptors, with C=O and N–H groups of the polymer, competing with intramolecular HBs within the selector and with selector–selectand intermolecular HBs.^{46,50} Indeed, with MeOH, hydrophobic interactions tend to be more favored compared with HBs, and the addition of water was expected to enhance hydrophobic interactions and increase capacity factors in accordance with a typical reversed-phase (RP) system.⁵¹

On this basis, 25 chromatographic systems generated by the combination of C-1, iC-5, A-1, iA-1, and iA-3 with the mixtures A–E, as MPs, were evaluated and characterized by k (Figure S1) and α (Figure S2) values toward ferrocenes **1–10** (Tables S3–S12). Baseline enantioseparations were obtained for compounds **1–8** and **10** with α values ranging from 1.10 to 11.41, whereas

TABLE 1 $V_{S,max}$ and $V_{S,min}$ values (au) associated with the main recognition sites (carbamate N–H, C=O, and Ar) of cellulose- and amylose-based selectors used in the study (DFT/B3LYP/def2TZVPP)

Chiral selector	Pendant group	$V_{S,max}$ (N–H)	$V_{S,min}$ (C=O)	$V_{S,min}$ (Ar)
CDMPC/ADMPC	3,5-Dimethylphenylcarbamate	0.0843	–0.0625	–0.0271
CDCPC	3,5-Dichlorophenylcarbamate	0.0990	–0.0536	–0.0066
ACMPC	3-Chloro-5-methylphenylcarbamate	0.0914	–0.0595	–0.0163

Abbreviations: ACMPC, amylose *tris*(3-chloro-5-methylphenylcarbamate); ADMPC, amylose *tris*(3,5-dimethylphenylcarbamate); CDCPC, cellulose *tris*(3,5-dichlorophenylcarbamate); CDMPC, cellulose *tris*(3,5-dimethylphenylcarbamate).

partial enantioseparation ($\alpha = 1.07$) was obtained only for **9**, with the system C-1/A. For compounds **1**, **3**, and **10**, baseline enantioseparations were achieved with *n*-hexanic and with aqueous-MeOH mixtures as MPs, but MeOH showed to exert a detrimental effect on the enantioseparation in these cases. Compounds **2** and **4–8** were baseline enantioseparated under all three elution modes, namely, *n*-hexanic mixtures, PO, and aqueous-organic elution conditions. Chromatographic conditions and parameters of the best enantioseparations obtained for compounds **1–8** and **10**, as a suitable compromise between a sufficiently high enantioselectivity value, a baseline resolution, and a run time as short as possible, are reported in Table 2 (see Figure S3 for chromatographic traces). For compounds **3–5**, **7**, and **8**, optimized enantioseparations were obtained by using chlorinated chiral columns (iA-3 or iC-5) with selectivity factors ranging from 1.46 to 2.92. Otherwise, for compounds **1**, **2**, **6**, and **10**, optimized enantioseparation methods were developed by using coated methylated chiral columns (C-1 or A-1) ($1.19 \leq \alpha \leq 2.13$). In the series of optimized enantioseparations, methanol-containing MPs were successfully used for compounds **1–4**, **6**, and **10** and *n*-hexanic mixtures for **5**, **7**, and **8**.

3.2 | Impact of analyte structure on enantioseparation

With the aim to evaluate the impact of the structural features of each analyte on its enantioseparability, the rate of baseline enantioseparations (*rb*s) was determined from the wealth of chromatographic results (Figure 3). In the frame of the 25 chromatographic systems explored in this study, *rb*s decreased following the order **7**, **8** (64%, 62%)

> **2** (32%) > **4,5** (28%) > **6** (16%) > **3,10** (12%) > **1** (8%) > **9** (0%). From this trend, some remarks emerged:

1. The 1,3-disubstituted ferrocenes showed high enantioseparability compared with the 1,2-disubstituted analogs (**7** > **4**, **8** > **5**, and **6** > **1**). Indeed, average retention factors (Figure S4a) and selectivity factors (Figure S4b) of **6**, **7**, and **8** ($1.56 \leq k \leq 11.88$; $1.05 \leq \alpha \leq 3.45$) were, in general, higher than those of **1**, **4**, and **5** ($0.65 \leq k \leq 1.62$; $1.05 \leq \alpha \leq 1.32$), respectively. This behavior could be caused by the fact that in the 1,3-pattern, both substituents are accessible to the selector, whereas the substituents are sterically constrained in 1,2-substituted derivatives. On the other hand, no relevant difference in terms of V_S values (Table S2), justifying the different *rb*s, was observed between 1,2- and 1,3-substituted derivatives;

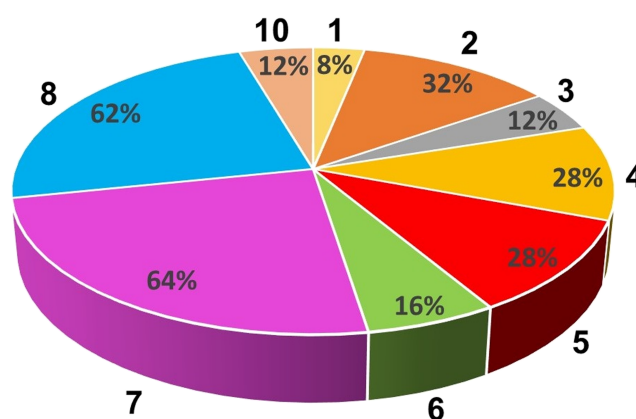


FIGURE 3 Rate of baseline enantioseparations of compounds **1–8** and **10** under multimodal elution conditions

TABLE 2 Chromatographic parameters (*t*, *k*, and α) for optimized baseline enantioseparations of *rac*-**1–8** and **10** on polysaccharide carbamate-based chiral columns under multimodal elution conditions

Compound	Column	MP	t_1 (min)	t_2 (min)	k_1	k_2	α	EEO
1	A-1	E	7.42	8.11	0.88	1.05	1.20	S-R
2	A-1	D	4.80	5.80	0.23	0.49	2.13	S-R
3	iA-3	E	6.79	8.09	0.71	1.03	1.46	S-R
4	iA-3	C	4.79	5.63	0.22	0.44	1.97	R-S
5	iC-5	A	7.22	9.29	0.95	1.51	1.59	S-R
6	A-1	C	7.91	8.68	1.05	1.25	1.19	R-S
7	iA-3	A	6.16	11.03	0.70	2.05	2.92	S-R
8	iA-3	A	7.34	10.12	1.03	1.80	1.75	S-R
10	C-1	D	6.18	7.60	0.55	0.90	1.65	Y-X

Note: The notation X or Y is reported for unknown absolute configuration.

Abbreviations: A, Hex/2-PrOH 95:5 v/v; A-1, Lux Amylose-1; B, Hex/2-PrOH/MeOH 95:2.5:2.5 v/v/v; C, MeOH 100%; C-1, Lux Cellulose 1; D, MeOH/water 95:5 v/v; E, MeOH:water 90:10 v/v; EEO, enantiomer elution order; iA-1, Lux i-Amylose-1; iA-3, Lux i-Amylose-3; iC-5, Lux i-Cellulose-5; MP, mobile phase.

- The ethynyl framework represents a key structural element given that the enantioselectivity decreased moving from **1** and **2** (*rbs*: 8% and 32%) to **9** and **10** (*rbs*: 0% and 12%), respectively. In terms of V_S values associated to nucleophilic and electrophilic regions, it is worth mentioning that, in **1** and **2**, the ethynyl group contributes to increase the electrophilic character of the iodine ($V_{S,\max}$ (I) = 0.0721 au (**1**) and 0.0755 au (**2**)), compared with the analogs **9** and **10** ($V_{S,\max}$ (I) = 0.0465 au (**9**) and 0.0529 au (**10**)), respectively. Interestingly, both *rbs* and positive $V_{S,\max}$ on iodine decrease along the bromiodo-substituted series **6** (*rbs* 16%, $V_{S,\max}$ (I) = 0.0737 au), **1** (*rbs* 8%, $V_{S,\max}$ (I) = 0.0721 au), and **9** (*rbs* 0%, $V_{S,\max}$ (I) = 0.0465 au). In addition, compound **2** presents higher electron density on the C≡N group ($V_{S,\min}$ (N) = -0.0721 au) and a more extended π -system compared with the analog **10** ($V_{S,\min}$ (N) = -0.0714 au);
- The presence of a π -extended system involving the second substituent of the iodoethynyl ferrocene impacts both retention and selectivity. Indeed, compounds **2**, **4**, **5**, **7**, and **8** showed average retention for both first and second eluted enantiomer, average selectivity, and *rbs* ($0.76 \leq k \leq 11.88$; $1.20 \leq \alpha \leq 3.45$; $28\% \leq rbs \leq 64\%$) higher compared with compounds **1**, **3**, **6**, **9**, and **10** ($0.54 \leq k \leq 1.64$; $1.01 \leq \alpha \leq 1.11$; $0\% \leq rbs \leq 16\%$);
- The EEO was determined for each enantioseparation, and the assignments are summarized in Table S5. *S-R* was the most frequent EEO, and only compound **2** retained this EEO in all chromatographic systems. Several cases of reversal of EEO dependent on analyte structure, selector structure, and MP type could be observed, but in general, they are not easy to explain. Compounds containing π -extended systems provided interesting cases of EEO. For instance, on C-1/A and C-1/B, all compounds showed *S-R* as EEO with the exception of **7** and **8** (*R-S*). Interestingly, by changing the *n*-hexanic mixtures to pure MeOH with the same chiral column (C-1/C), only compound **8** retained the *R-S* sequence as EEO, whereas compound **7** showed MP-dependent EEO reversal to *S-R*, despite the structural similarity of the two analytes. Compound **5** showed the *S-R* elution order on all amylose-based selectors with mixture A, but adding 2.5% MeOH provided EEO reversal to *R-S* on the same selectors. Again, only for compound **5**, a reversal of elution order was observed on immobilized iA-1 (*R-S*) compared with the coated A-1 (*S-R*) by using MeOH or the aqueous mixture D as MPs. The same phenomenon was not observed with *n*-hexanic mixtures (mixtures A and B).

3.3 | Impact of selector structure on enantioseparation

Among the chiral columns used in this study, better results were obtained on the A-1 and iA-3, each column providing baseline enantioseparations for seven compounds. C-1 was also able to enantioseparate six compounds, whereas iC-5 and iA-1 provided baseline enantioseparations only for compounds **2**, **4**, **5**, and **10**, and **7** and **8**, respectively (Figure S6). Compounds **2** and **10** containing the C≡N group as a strong HB acceptor showed very high retention on the iC-5 ($5.39 \leq k \leq 6.29$) with *n*-hexanic mixtures but moderate selectivity on this chiral column ($\alpha = 1.11$ (**2**), 1.15 (**10**)). Thus, the acidic amidic hydrogen of the CDCPC strongly contributes to determine the affinity of the analyte toward the selector participating in the C≡N...H-N HB but less to enantioselectivity.

Among all compounds, 1,3-disubstituted **7** and **8** showed an interesting behavior with very high affinity for the amylose-based selectors by using methanol-containing MPs (Tables S9 and S10). The same behavior was not observed for the 1,2-analogs **4** and **5**.

3.4 | Enantioseparation of compounds 7 and 8: CDMPC versus ADMPC

As shown in Figure 4, 1,3-disubstituted ferrocenes **7** and **8** showed a complementary behavior on C-1 as the MP changes, and in both cases, two mechanisms seem to control enantioseparation on this column depending on MP polarity:

- A mechanism based on polar interactions occurring with mixture A, which proved to be more effective, in terms of selectivity, for compound **8** (R = naphthyl) ($\alpha = 1.25$) compared with derivative **7** (R = Ph) ($\alpha = 1.08$). The addition of methanol to mixture A, or the use of pure MeOH as MP, appeared to be detrimental for the enantioseparation in both cases;
- A mechanism occurring under hydrophobic conditions when increasing amounts of water (5% and 10%) were added to the MP consisting of pure methanol. In these cases, the separation system behaves as a typical reversed-phase system, and selectivity factors increased with increasing amount of water.⁴⁶ Under these conditions, compound **7** ($\alpha = 1.19$) was enantioseparated better than compound **8** ($\alpha = 1.09$).

Interestingly, for compound **7**, the transition between the two mechanisms is associated with a MP-dependent reversal of EEO, which is *R-S* with A and B

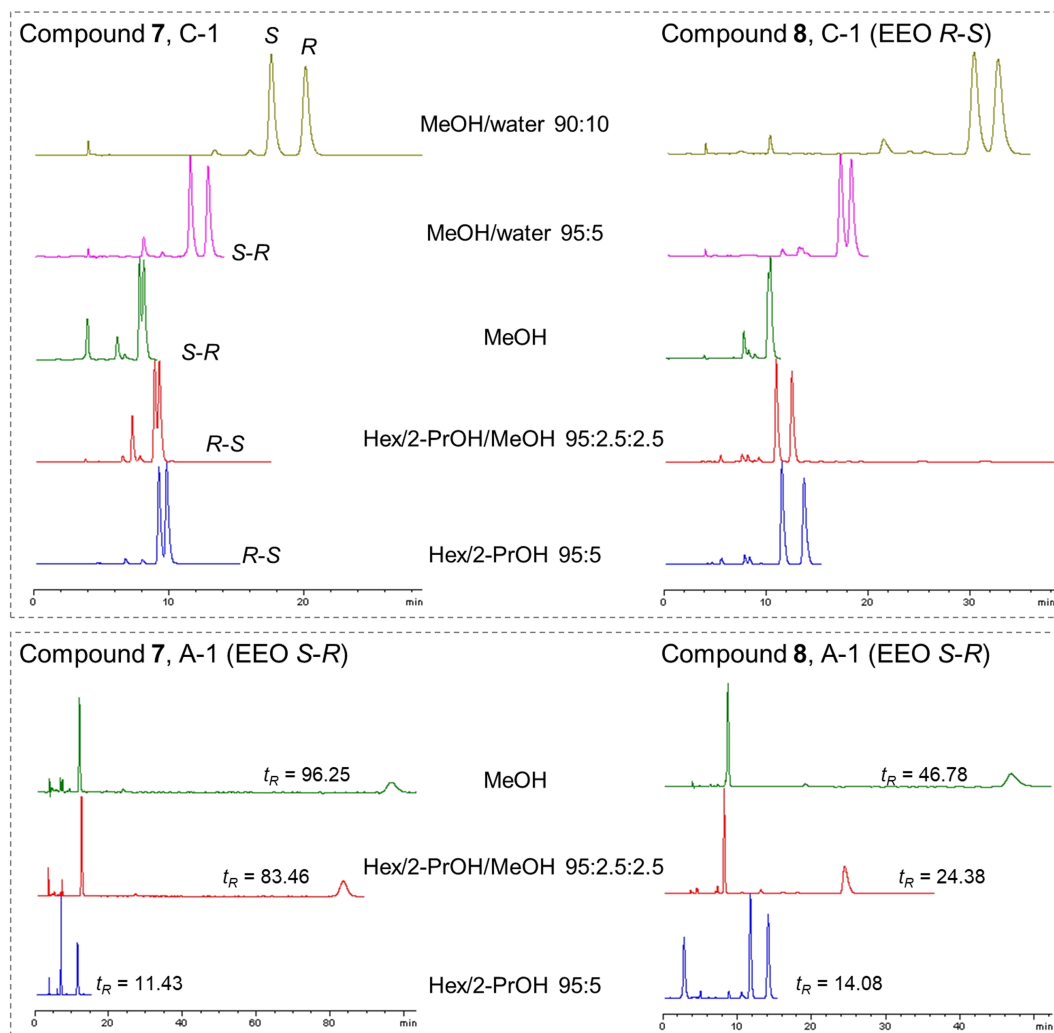


FIGURE 4 Comparison of the enantioseparation traces of compounds 7 and 8 on C-1 and A-1 under multimodal elution conditions

as MPs and *S-R* with pure methanol and aqueous mixtures D and E. Otherwise, the naphthyl derivative 8 retained the same *R-S* elution sequence with all MPs (A–E).

The features of the enantioseparations of compounds 7 and 8 on A-1 were shown to be completely different (Figure 4). In these cases, with mixture A, the phenyl derivative 7 was enantioseparated better ($\alpha = 2.27$) than compound 8 ($\alpha = 1.29$), showing an opposite trend compared with the enantioseparations on CDMPC, also in terms of EEO (CDMPC: *R-S*; ADMPC: *S-R*). On the amylose-based selector, the use of methanol-containing MPs such as B and C increased retention and selectivity producing large enantioseparation for both compounds 7 ($\alpha_B = 8.87$; $\alpha_C = 11.41$) and 8 ($\alpha_B = 4.50$; $\alpha_C = 8.92$). In particular, for compound 7, the addition of only 2.5% MeOH to the binary mixture A caused the increase of the retention time of the second eluted (*R*)-enantiomer from 11.43 min ($k_2 = 2.34$, $\alpha = 2.27$) to 83.46 min ($k_2 = 22.59$,

$\alpha = 8.87$) and a further increase to 96.25 min ($k_2 = 23.95$, $\alpha = 11.41$) by using pure MeOH as MP. The effect occurred in less degree for compound 8, the retention time of the second eluted enantiomer changing from 14.08 min ($k_2 = 3.12$, $\alpha = 1.29$) to 24.38 ($k_2 = 5.89$, $\alpha = 4.50$) and 46.6 min ($k_2 = 11.13$, $\alpha = 8.92$) with A, B, and C as MPs, respectively.

The application of van't Hoff analysis allowed for identifying different thermodynamic profiles for compounds 7 and 8 as the cause of the different selectivity observed by changing the ADMPC to CDMPC. Thus, retention and selectivity of compounds 7 and 8 on C-1 and A-1 with Hex/2-PrOH 95:5 v/v as MP were determined at different temperatures from 5°C to 45°C in 5°C increments (Table S13). The thermodynamic quantities derived from van't Hoff plots (Figure S7) are reported in Table S14. The enantioseparations of both analytes on C-1 were shown to be enthalpy driven with $T_{\text{iso}} = 147^\circ\text{C}$ and 85°C for 7 and 8, respectively. Otherwise, the

enantioseparation of **8** on A-1 is entropy-driven ($|\Delta\Delta S^\circ| > |\Delta\Delta H^\circ|$), and a $T_{\text{iso}} = -37^\circ\text{C}$ was calculated in this case. An enthalpy-driven process also occurred ($|\Delta\Delta S^\circ| < |\Delta\Delta H^\circ|$) for the enantioseparation of **7** on A-1, where the difference between the free energies associated to the transfer of the enantiomers from the MP to the selector surfaces is essentially due to a negative enthalpy contribution ($-281.3\text{ cal}\cdot\text{mol}^{-1}$), whereas the entropy term is positive and close to zero ($0.78\text{ cal}\cdot\text{K}^{-1}\cdot\text{mol}^{-1}$). Indeed, the enantioselectivity is almost independent of the temperature variation. Moving from C-1 to A-1, an increase of the entropy contribution to enantioselection could be determined by comparing the values of the thermodynamic ratio $Q = \Delta\Delta H^\circ / (298 \times \Delta\Delta S^\circ)$: **7**, 1.41 (C-1) \rightarrow 1.21 (A-1); **8**, 1.20 (C-1) \rightarrow 0.79 (A-1).

Large separations for compounds **7** and **8** were also observed on iA-1 (Figures S8 and S9) and iA-3 (Figures S10 and S11), but not with cellulose-based selectors, showing that the high affinity of the second eluted enantiomers of these compounds toward the selectors is mainly determined by the features of backbone with methanol-containing MP, thus occurring under hydrophobic conditions. With the aim to confirm this feature, we explored the impact of adding polar and nonpolar components to the MP on the retention of the second (*R*)-enantiomer of compounds **7** and **8** by using iA-1 (Figures S8 and S9). Considering that solvents favor and disfavor hydrophobic and polar interactions, respectively, following the order $\text{ACN} < 2\text{-PrOH} < \text{MeOH} < \text{water}$, changing the aqueous mixture D to MeOH/2-PrOH, and MeOH/ACN as MPs, caused a decrease in the retention

of the (*R*)-enantiomer of **7** from 113.10 min to 23.28 and 18.38 min, respectively. Otherwise, by adding 5% water to pure ACN, retention time of the (*R*)-enantiomer increased from 15.12 to 26.89 min. On this basis, by changing MeOH to ACN in mixture D, a drop of retention time of the (*R*)-enantiomer from 113.10 to 26.89 min was observed. On the other hand, the retention factors of the first eluted (*S*)-enantiomer ($0.56 \leq k_2 \leq 3.50$) showed to be less influenced by the polarity of the MP compared with the (*R*)-enantiomer ($2.56 \leq k_2 \leq 27.79$). A similar trend was obtained for compound **8**. The evaluation of the “dance” of the second peak on the timescale under multimodal conditions (Figures S8 and S9) allowed to confirm that the high affinity of the analyte toward amylose-based selectors actually originates from hydrophobic conditions.

With the aim to explore the binding mechanism of (*R*)-**7** at the molecular level,^{48,52–55} a MD simulation was performed by using the (*R*)-**7** as selectand, an ADMPC nonamer as selector, and MeOH as a virtual solvent (Figure 5). The modeling of the experimental binding confirmed that the (*R*)-enantiomer of compound **7** penetrates deeply in the groove of the selector (Figure 5A). The selectand remained blocked during 100 ns of MD and confined in a hydrophobic cavity, which appeared to be profiled by six aromatic rings of the selector (Figure 5B). Interestingly, an HB between the π -ethynyl cloud and the amidic hydrogen of the selector ($d = 2.347\text{ \AA}$) was observed to contribute to the binding of the (*R*)-enantiomer into the polymer groove, confirming the pivotal role of this structural element on enantioseparation.

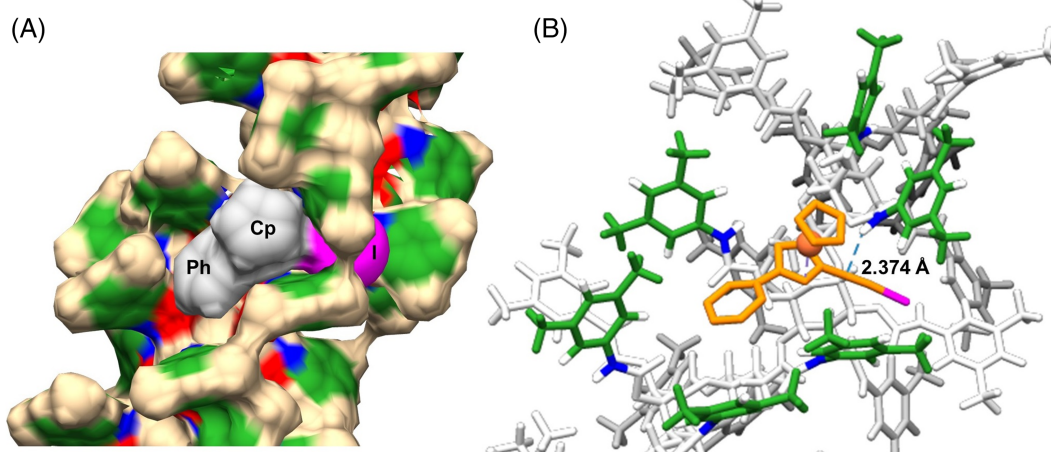


FIGURE 5 Representative snapshot from the simulated molecular dynamics trajectories (100 ns) of (*R*)-**7** complex with amylose tris (3,5-dimethylphenylcarbamate) (ADMPC) (solvent box, MeOH): (A) electron density surface (legend colors: green, aromatic ring; red, C=O; blue, N-H; gray, Ph + Cp + C≡C of (*R*)-**7**; magenta, iodine) and (B) tube model of the (*R*)-**7**/ADMPC complex (legend colors: orange, Ph + Cp + Fe + C≡C of (*R*)-**7**; magenta, iodine; green, aromatic rings featuring and delimiting the hydrophobic binding cavity of ADMPC)

4 | CONCLUSION

In this study, the enantioseparation of ferrocenes **1–10** has been explored systematically, and as a result, methods for baseline enantioseparations were successfully developed for nine compounds with selectivity factors ranging from 1.20 to 2.92. Otherwise, 1-bromo-2-iodo-ferrocene (**9**) could be only partially enantioseparated, confirming that the enantioseparation of small nonpolar planar chiral ferrocenes remains rather challenging due to the inherent structural inability of the enantiomers of this type of molecular systems to be enantiodifferentiated. In most cases, amylose-based CSPs provided better enantioseparation performances compared with cellulose-based ones. Due to the hydrophobic feature of the ferrocenes used in this study as analytes, aqueous methanol-containing MPs allowed for improving enantioseparation performances in several cases.

The impact of π -extended clouds on the enantioseparations was clearly demonstrated, compounds **7** and **8** providing interesting trends and behaviors as both selector and MP features changes. Interestingly, the addition of small (2.5%) percentages of methanol to the Hex/2-PrOH 95:5 increased significantly the affinity of the second eluted enantiomers of compounds **7** and **8**, producing large enantioseparations on amylose-based selectors ranging from 4.69 to 11.41 and from 4.50 to 8.92, respectively.

MD simulations disclosed (a) the confinement of the analyte in a hydrophobic cavity deeply inside the ADMPC groove and (b) the stabilization of the selector–selectand complex exerted by an HB between the ethynyl π -cloud and the amidic hydrogen of the selector, as the molecular basis underlying the high affinity of analytes **7** and **8** toward amylose-based selectors.

ACKNOWLEDGMENTS

We thank CNR, University of Strasbourg, and CNRS for financial support. M. P. B. acknowledges to Generalitat Valenciana and European Social Fund for the contribution to the contract ACIF/2019/158 and to the research stay BEFPI/2021/073.

DATA AVAILABILITY STATEMENT

Data are available on request from the authors.

ORCID

Bezhan Chankvetadze  <https://orcid.org/0000-0003-2379-9815>

Paola Peluso  <https://orcid.org/0000-0003-3489-3428>

REFERENCES

- Fabbrizzi L. The ferrocenium/ferrocene couple: a versatile redox switch. *Chem Texts*. 2011;6(4):1-20. doi:10.1007/s40828-020-00119-6
- Wilkinson G, Rosenblum M, Whiting MC, Woodward RB. The structure of iron bis-cyclopentadienyl. *J Am Chem Soc*. 1952;74(8):2125-2126. doi:10.1021/ja01128a527
- Lotz M, Ireland T, Tappe K, Knochel P. Preparation of new chiral borane-protected P,N-ferrocenyl ligands via a methoxy directed ortho-lithiation. *Chirality*. 2000;12:389-395. doi:10.1002/(SICI)1520-636X(2000)12:5/6<389::AID-CHIR16>3.0.CO;2-S
- Astruc D. Why is ferrocene so exceptional? *Eur J Inorg Chem*. 2017;1:6-29. doi:10.1002/ejic.201600983
- Tazi M, Hedidi M, Erb W, et al. Fluoro- and chloroferrocene: from 2- to 3-substituted derivatives. *Organometallics*. 2018;37(14):2207-2221. doi:10.1021/acs.organomet.8b00384
- Mamane V, Peluso P, Aubert E, et al. Disubstituted ferrocenyl iodo- and chalcogenoalkynes as chiral halogen and chalcogen bond donors. *Organometallics*. 2020;39(21):3936-3950. doi:10.1021/acs.organomet.0c00633
- Ravutsov M, Dobrikov GM, Dangalov M, et al. 1,2-Disubstituted planar chiral ferrocene derivatives from sulfonamide-directed ortho-lithiation: synthesis, absolute configuration, and chiroptical properties. *Organometallics*. 2021;40(5):578-590. doi:10.1021/acs.organomet.0c00712
- Dai LX, Tu T, You SL, Deng WP, Hou XL. Asymmetric catalysis with chiral ferrocene ligands. *Acc Chem Res*. 2003;36(9):659-667. doi:10.1021/ar020153m
- Cunningham L, Benson A, Guiry PJ. Recent developments in the synthesis and applications of chiral ferrocene ligands and organocatalysts in asymmetric catalysis. *Org Biomol Chem*. 2020;18(46):9329-9370. doi:10.1039/d0ob01933j
- Aubert E, Doudouh A, Wenger E, et al. Chiral ferrocenyl-iodotriazoles and -iodotriazoliums as halogen bond donors. Synthesis, solid state analysis and catalytic properties. *Eur J Inorg Chem*. 2021; submitted. In press, doi:10.1002/ejic.202100927
- Patra M, Gasser G. The medicinal chemistry of ferrocene and its derivatives. *Nat Rev Chem*. 2017;1(9):0066. doi:10.1038/s41570-017-0066
- Chuard T, Deschenaux R. Functional liquid-crystalline materials based on ferrocene. *Chimia*. 2003;57(10):597-600. doi:10.2533/000942903777678803
- Vollmann M, Butenschön H. Synthesis of a functionalized dialkynylferrocene for molecular electronics. *Comptes Rendus Chimie*. 2005;8(8):1282-1285. doi:10.1016/j.crci.2005.02.019
- Benecke J, Grape ES, Fuß A, et al. Polymorphous indium metal–organic frameworks based on a ferrocene linker: redox activity, porosity, and structural diversity. *Inorg Chem*. 2020;59(14):9969-9978. doi:10.1021/acs.inorgchem.0c01124
- Peng L, Feng A, Huo M, Yuan J. Ferrocene-based supramolecular structures and their applications in electrochemical responsive systems. *Chem Commun*. 2014;50(86):13005-13014. doi:10.1039/c4cc05192k
- Lim JYC, Beer PD. A halogen bonding 1,3-disubstituted ferrocene receptor for recognition and redox sensing of azide. *Eur J Inorg Chem*. 2017;2:220-224. doi:10.1002/ejic.201600805

17. Ding F, Chen S, Wang H. Computational study of ferrocene-based molecular frameworks with 2,5-diethylpyridine as a chemical bridge. *Materials*. 2010;3(4):2668-2683. doi:10.3390/ma3042668
18. Schmiel SF, Butenschön H. New π -extended 1,1'-disubstituted ferrocenes with thioate and dithioate end groups. *Eur J Org Chem*. 2021;2021(17):2388-2401. doi:10.1002/ejoc.202100335
19. Bennett TLR, Wilkinson LA, Lok JMA, O'Toole RCP, Long NJ. Synthesis, electrochemistry, and optical properties of highly conjugated alkynyl-ferrocenes and -biferrocenes. *Organometallics*. 2021;40(8):1156-1162. doi:10.1021/acs.organomet.1c00098
20. Getty SA, Engtrakul C, Wang L, et al. Near-perfect conduction through a ferrocene-based molecular wire. *Phys Rev B*. 2005;71(24):241401 doi:10.1103/PhysRevB.71.241401
21. Urbano A, del Hoyo AM, Martínez-Carrión A, Carreño MC. Asymmetric synthesis and chiroptical properties of enantiopure helical ferrocenes. *Org Lett*. 2019;21(12):4623-4627. doi:10.1021/acs.orglett.9b01522
22. Dumele O, Wu D, Trapp N, Goroff N, Diederich F. Halogen bonding of (iodoethyl)benzene derivatives in solution. *Org Lett*. 2014;16(18):4722-4725. doi:10.1021/ol502099j
23. Aakeröy CB, Wijethunga TK, Desper J, Đakovic M. Crystal engineering with iodoethylnitrobenzenes: a group of highly effective halogen-bond donors. *Cryst Growth des*. 2015;15(8):3853-3861. doi:10.1021/acs.cgd.5b00478
24. Peluso P, Mamane V, Aubert E, et al. Insights into halogen bond-driven enantioseparations. *J Chromatogr A*. 2016;1467:228-238. doi:10.1016/j.chroma.2016.06.007
25. Peluso P, Mamane V, Dallochio R, et al. Polysaccharide-based chiral stationary phases as halogen bond acceptors: a novel strategy for detection of stereoselective σ -hole bonds in solution. *J Sep Sci*. 2018;41(6):1247-1256. doi:10.1002/jssc.201701206
26. Peluso P, Gatti C, Dessì A, et al. Enantioseparation of fluorinated 3-arylthio-4,4'-bipyridines: insights into chalcogen and π -hole bonds in high-performance liquid chromatography. *J Chromatogr A*. 2018;1567:119-129. doi:10.1016/j.chroma.2018.06.060
27. Peluso P, Dessì A, Dallochio R, et al. Enantioseparation of 5,5'-dibromo-2,2'-dichloro-3-selanyl-4,4'-bipyridines on polysaccharide-based chiral stationary phases: exploring chalcogen bonds in liquid-phase chromatography. *Molecules*. 2021;26(1):221 doi:10.3390/molecules26010221
28. Yamazaki Y, Morohashi N, Hosono K. High-performance liquid chromatographic determination of optical purity of planar chiral organometallic compounds resolved by enzymic transformations. *J Chromatogr A*. 1991;542:129-136. doi:10.1016/S0021-9673(01)88753-7
29. Tsukazaki M, Tinkl M, Roglans A, Chapell BJ, Taylor NJ, Snieckus V. Direct and highly enantioselective synthesis of ferrocenes with planar chirality by (-)-sparteine-mediated lithiation. *J Am Chem Soc*. 1996;118(3):685-686. doi:10.1021/ja953246q
30. Thorat RA, Jain S, Sattar M, Yadav P, Mandhar Y, Kumar S. Synthesis of chiral-substituted 2-aryl-ferrocenes by the Catellani reaction. *J Org Chem*. 2020;85(23):14866-14878. doi:10.1021/acs.joc.0c01360
31. Patti A, Pedotti S, Sanfilippo C. Comparative HPLC enantioseparation of ferrocenylalcohols on two cellulose-based chiral stationary phases. *Chirality*. 2007;19(5):344-351. doi:10.1002/chir.20386
32. Ogasawara M, Enomoto Y, Uryu M, Yang X, Kataoka A, Ohnishi A. Application of polysaccharide-based chiral HPLC columns for separation of nonenantiomeric isomeric mixtures of organometallic compounds. *Organometallics*. 2019;38(2):512-518. doi:10.1021/acs.organomet.8b00819
33. Okamoto Y, Kawashima M, Hatada K. Useful chiral packing materials for high-performance liquid chromatographic resolution of enantiomers: phenylcarbamates of polysaccharides coated on silica gel. *J Am Chem Soc*. 1984;106(18):5357-5359. doi:10.1021/ja00330a057
34. Okamoto Y, Kawashima M, Yamamoto K, Hatada K. Useful chiral packing materials for high-performance liquid chromatographic resolution. Cellulose triacetate and tribenzoate coated on microporous silica gel. *Chem Lett*. 1984;13(5):739-742. doi:10.1246/cl.1984.739
35. Li W, Zhang W, Wang X, Dou J, Chen L, Li Y. Chiral separation of novel chiral tetrahedron-type clusters on a cellulose tris(3,5-dimethylphenylcarbamate) chiral stationary phase. *Anal Chim Acta*. 2003;495(1-2):77-83. doi:10.1016/j.aca.2003.08.038
36. Zhu X, Cai Y, Zhang W, Chen L, Li Y. Enantioseparation of novel chiral heterometal tetrahedral clusters by high-performance liquid chromatography. *J Chromatogr A*. 2003;1002(1-2):231-236. doi:10.1016/S0021-9673(03)00655-1
37. Wang X, Li W, Zhao Q, Li Y, Chen L. Normal-phase HPLC enantioseparation of novel chiral metal tetrahedron-type clusters on an amylose-based chiral stationary phase. *Anal Sci*. 2005;21(2):125-128. doi:10.2116/analsci.21.125
38. Gallinella B, Bucciarelli L, Zanitti L, Ferretti R, Cirilli R. Direct separation of the enantiomers of oxaliplatin on a cellulose-based chiral stationary phase in hydrophilic interaction liquid chromatography mode. *J Chromatogr A*. 2014;1339:210-213. doi:10.1016/j.chroma.2014.02.071
39. Citti C, Battisti UM, Ciccarella G, et al. Analytical and preparative enantioseparation and main chiroptical properties of Iridium (III) bis(4,6-difluorophenylpyridinato)picolinato. *J Chromatogr A*. 2016;1467:335-346. doi:10.1016/j.chroma.2016.05.059
40. Dayaker G, Sreeshailam A, Chevallier F, Roisnel T, Krishna PR, Mongin F. Deprotonative metallation of ferrocenes using mixed lithium-zinc and lithium-cadmium combinations. *Chem Commun*. 2010;46(16):2862-2864. doi:10.1039/B924939G
41. Frisch MJ, Trucks GW, Schlegel HB, et al. *Gaussian 09, Revision B.01*. C.T. Wallingford: Inc. Gaussian; 2010.
42. Lu T, Chen F. Multiwfn: a multifunctional wavefunction analyzer. *J Comput Chem*. 2012;33(5):580-592. doi:10.1002/jcc.22885
43. Lu T, Chen F. Quantitative analysis of molecular surface based on improved Marching Tetrahedra algorithm. *J Mol Graph Model*. 2012;38:314-323. doi:10.1016/j.jmkgm.2012.07.004
44. Chankvetadze B. Recent trends in preparation, investigation and application of polysaccharide-based chiral stationary phases for separation of enantiomers in high-performance liquid chromatography. *Trends Anal Chem*. 2020;122:115709. doi:10.1016/j.trac.2019.115709
45. Peluso P, Sechi B, Lai G, et al. Comparative enantioseparation of chiral 4,4'-bipyridine derivatives on coated and immobilized

- amylose-based chiral stationary phases. *J Chromatogr A*. 2020; 1625:461303. doi:10.1016/j.chroma.2020.461303
46. Chankvetadze B, Yamamoto C, Okamoto Y. Enantioseparation of selected chiral sulfoxides using polysaccharide-type chiral stationary phases and polar organic, polar aqueous-organic and normal-phase eluents. *J Chromatogr A*. 2001;922(1-2):127-137. doi:10.1016/S0021-9673(01)00958-X
47. Chankvetadze B. Recent developments on polysaccharide-based chiral stationary phases for liquid-phase separation of enantiomers. *J Chromatogr A*. 2012;1269:26-51. doi:10.1016/j.chroma.2012.10.033
48. Zhao B, Oroskar PA, Wang X, et al. The composition of the mobile phase affects the dynamic chiral recognition of drug molecules by the chiral stationary phase. *Langmuir*. 2017; 33(42):11246-11256. doi:10.1021/acs.langmuir.7b02337
49. Horváth S, Németh G. Hysteresis of retention and enantioselectivity on amylose tris(3,5-dimethylphenylcarbamate) chiral stationary phases in mixtures of 2-propanol and methanol. *J Chromatogr A*. 2018;1568:149-159. doi:10.1016/j.chroma.2018.07.033
50. Chankvetadze B. Polysaccharide-based chiral stationary phases for enantioseparations by high-performance liquid chromatography: an overview. In: Scriba GKE, ed. *Chiral separations: methods and protocols, Methods in molecular biology*. Vol. 1985. Springer Science + Business Media, LLC, part of Springer Nature; 2019:93-126.
51. Shedania Z, Kakava R, Volonterio A, Farkas T, Chankvetadze B. Separation of enantiomers of chiral sulfoxides in high-performance liquid chromatography with cellulose-based chiral selectors using methanol and methanol-water mixtures as mobile phases. *J Chromatogr A*. 2018;1557:62-74. doi:10.1016/j.chroma.2018.05.002
52. Dallochio R, Dessì A, Solinas M, et al. Halogen bond in high-performance liquid chromatography enantioseparations: description, features and modelling. *J Chromatogr A*. 2018; 1563:71-81. doi:10.1016/j.chroma.2018.05.061
53. Peluso P, Mamane V, Dallochio R, Dessì A, Cossu S. Noncovalent interactions in high-performance liquid chromatography enantioseparations on polysaccharide-based chiral selectors. *J Chromatogr A*. 2020;1623:461202. doi:10.1016/j.chroma.2020.461202
54. Dallochio R, Sechi B, Dessì A, et al. Enantioseparations of polyhalogenated 4,4'-bipyridines on polysaccharide-based chiral stationary phases and molecular dynamics simulations of selector-selectand interaction. *Electrophoresis*. 2021;42(17-18): 1853-1863. doi:10.1002/elps.202100049
55. Varfaj I, Di Michele A, Ianni F, et al. Enantioseparation of novel anti-inflammatory chiral sulfoxides with two cellulose dichlorophenylcarbamate-based chiral stationary phases and polar-organic mobile phase(s). *J Chromatogra Open*. 2021;1: 100022. doi:10.1016/j.jcoa.2021.100022

SUPPORTING INFORMATION

Additional supporting information may be found in the online version of the article at the publisher's website.

How to cite this article: Dessì A, Sechi B, Dallochio R, et al. Comparative enantioseparation of planar chiral ferrocenes on polysaccharide-based chiral stationary phases. *Chirality*. 2022;34(4): 609-619. doi:10.1002/chir.23417